

**Thermoplastic polyurethane with controllable degradation
and critical anti-fouling properties**

Journal:	<i>Biomaterials Science</i>
Manuscript ID	BM-ART-11-2020-001967.R1
Article Type:	Paper
Date Submitted by the Author:	30-Nov-2020
Complete List of Authors:	Wang, Huifeng; University of Illinois at Chicago Liu, Xuan; University of Illinois at Chicago Christiansen, Daniel ; University of Illinois at Chicago Fattahpour, Seyyedfaridoddin; University of Illinois at Chicago Wang, Kun; University of Illinois at Chicago Song, Haiqing; University of Illinois at Chicago Mehraeen, Shafigh; University of Illinois at Chicago Cheng, Gang; University of Illinois at Chicago

Thermoplastic polyurethane with controllable degradation and critical anti-fouling properties

Huifeng Wang,¹ Xuan Liu,¹ Daniel Edward Christiansen,¹ Seyyedfaridoddin Fattahpour,¹ Kun Wang,¹ Haiqing Song,¹ Shafiqh Mehraeen,¹ Gang Cheng*¹

¹Department of Chemical Engineering, University of Illinois at Chicago, Chicago, IL 60607, United States

Corresponding Author

* Dr. Gang Cheng E-mail: gancheng@uic.edu

Department of Chemical Engineering, the University of Illinois at Chicago, Chicago, Illinois 60607, USA

Homepage: <https://gancheng.people.uic.edu/>

Keywords: Zwitterionic, degradable, carboxybetaine, polyurethane, anti-fouling surface, elastomer

Abstract

Bioresorbable polymers, including polyesters and polypeptides, are being widely used in the medical field. However, these materials still suffer from some long-standing challenges, such as material-induced blood coagulation, foreign body response, non-adjustable degradation rate, and absence of elastic properties. In this work, we explored a new approach to address these challenges by incorporating critical anti-fouling, improved mechanical and controllable degradation properties into the existing bioresorbable polymers. We synthesized a set of zwitterionic thermoplastic polyurethanes, which consist of degradable polycaprolactone diols as soft segments and faster hydrolyzable carboxybetaine (CB) diols as chain extenders. Differential scanning calorimetry and temperature sweep rheology revealed thermal transition performance and thermoplastic behavior of the polymers. The calorimetric study observed that CB-based chain extender played a critical role in the crystallization process by affecting the structure and crystallization temperature. Cell attachment study demonstrated that the degradable zwitterionic polyurethane surfaces highly resist cell attachment even after being submerged in 100% fetal bovine serum for two weeks. The gold standard PEG-based degradable polyurethane showed the initial resistance to the cell attachment for one day and then failed after three days. This work clearly shows that the adaption of existing materials with slightly better anti-fouling properties is unlikely to solve these long-lasting challenges. Our design approach and the material platform with critical anti-fouling properties and other desired tunable properties show the potential to address these complications associated with existing bioresorbable polymers. This method can be adapted to design customized bioresorbable polymers for a wide range of applications, including implantable biomedical devices and drug delivery.

1. Introduction

The field of implantable medical devices has grown exponentially over the last half-century, with millions in the U.S. alone having at least one in their body. These devices have seen significantly improved safety and performance. Still, material-induced thrombosis,¹ implant-associated infections² and foreign body response (FBR),³ remain significant challenges, which decrease the effectiveness and service life of the devices and cause life-threatening complications.^{4, 5} Over one million implantable polymeric medical device-related incidents (i.e., injuries, disabilities, and death) have involved such phenomenon, as reported in 2018 by the US Food and Drug Administration. Previous studies have observed that material-associated thrombosis,¹ biofilm formation,² and FBR³ share a similar initiating process: the initial adsorption of biomolecules causes the attachment of platelets, macrophages/monocytes, or microbes and subsequently results in thrombosis, FBR, or infection. To address these long-standing challenges in medicine, the development of effective materials with a pronounced resistance to non-specific protein adsorption and cell adhesion is desirable.^{3, 6, 7}

Among all materials, thermoplastic biodegradable polymers are particularly attractive for use as medical implants, sutures, tissue engineering scaffolds, and drug delivery vehicles, owing to their ability to break down within the body naturally. This capability circumvents the need for a second procedure to remove them and prevents their accumulation in the body. The thermoplasticity allows materials to be conveniently fabricated by the commonly-used processing methods, such as extrusion, injection molding, and 3D printing. A few common materials belonging to this category are poly(caprolactone) (PCL),⁸ poly(lactic acid) (PLA),^{9, 10} poly(lactic-co-glycolic acid) (PLGA),¹¹ poly(anhydride-ester),¹² and polyurethane (PU) (a certain combination of the previous three).¹³⁻¹⁶ It was expected initially that degradable materials would resist FBR and thrombosis. However, studies revealed that PLA¹⁷ and PCL¹⁸ trigger obvious FBR¹⁹ and thrombosis.²⁰ Degradable material-associated FBR, thrombosis, and infection are mainly the result of the biomacromolecule adsorption rate being higher than the material degradation rate and the hydrophobic nature of these materials.²¹ In addition to their lack of anti-fouling properties, these

degradable materials also exhibit uncontrollable mechanical and degradation properties. For the aforementioned challenges, degradable materials were combined with other materials possessing the desired anti-fouling properties. Among these added materials, polyurethane is of great interest for its unique tunability or the convenience of controlling the physical and chemical properties.²² Because of the high density of strong hydrogen bond-forming urethane groups, polyurethane exhibits desirable traits, such as good wettability, strength, and elasticity, for medical applications.^{23, 24} Many polyurethanes have shown lower protein adsorption than other hydrophobic polymers, including polyethylene, polyvinyl chloride, etc. However, their anti-fouling properties are still insufficient in complex biological environments (such as blood and body fluids).²⁵ For these reasons, polyurethane is a suitable starting material for further studies on improving the anti-fouling and mechanical properties while maintaining the biodegradability of the bioresorbable polymers.²⁶

We hypothesized that zwitterionic moieties are essential to provide critical anti-fouling properties to address the biofouling-related challenges of degradable polymeric materials. Previous studies reported a competitive class of hydrophilic polymers as ultra-low fouling materials,²⁷ including poly(hydroxyethyl methacrylate),²⁸ poly(ethylene glycol) (PEG).^{29, 30} PEG exhibited anti-fouling properties against a fibrinogen (Fg) solution. However, Ladd *et al.* observed that 100% human blood plasma adsorbs on the PEG surface at 7 ng/cm². That value is higher than the undetectable adsorption level on zwitterionic poly(carboxybetaine methacrylate) (PCBMA) measured by a surface plasmon resonance (SPR) sensor with a detection limit of 0.3 ng/cm².³¹ Furthermore, several recent studies also observed PEG triggering FBR^{32, 33} and immune response.^{34, 35} Compared to PEG, zwitterionic materials (including poly(carboxybetaine),^{36, 37} poly(sulfobetaine),^{38, 39} and poly(phosphocholine)⁴⁰), which carry balanced cations and anions, demonstrated more consistent anti-fouling properties. An earlier study by Dr. Jiang and co-workers demonstrated that polycarboxybetaine could reduce over 94% of biofilm for ten days compared to the unmodified glass.⁴¹ The charged cations and anions in the existing zwitterionic polymers lead to the high polarity and high glass transition temperature.

These polymers can not be processed as thermoplastics by commonly-used polymer processing techniques. Due to their high polarity and solubility in water, the linear zwitterionic materials exhibit relatively low modulus and unsatisfactory elasticity, limiting their utilities.⁴²⁻⁴⁴ To address this challenge, an elastic and nondegradable zwitterionic polymer was developed.⁴⁵ Recently, we invented an innovative method to enable zwitterionic polyurethanes (PUs) to carry unmatched performance in resisting biofilm growth of *Pseudomonas aeruginosa* and *Staphylococcus epidermidis* for six months, blood adsorption, and cell attachment while simultaneously having tunable mechanical properties.^{46, 47} The direct incorporation of highly polar and nondegradable zwitterionic moieties to degradable, less polar polymers results in phase separation, undesired mechanical properties and partial degradability. Such materials also require significant modifications, which requires postprocessing functionalization of PU with a zwitterionic polymer,⁴⁸⁻⁵⁰ and it will significantly increase the cost and change the processability of PU. to the processing methods. Thus, new strategies that can provide degradable materials with critical anti-fouling properties at the biointerfaces, thermoplasticity, controllable degradation rate, and tunable mechanical properties are required.

Herein, we invented a new strategy to incorporate critical anti-fouling properties, thermoplasticity, controllable degradation rate, and tunable mechanical properties into one material. We designed and synthesized a series of degradable elastomers, polyurethane-poly(carboxybetaine-*co*-hexamethylene diisocyanate-*co*-PCL) (PCBDUs), with improved mechanical properties, tunable degradation rate, and critical anti-fouling properties. PCBDUs carry different amounts of faster hydrolyzable CB diol chain extenders and slower degradable PCL soft domains in polymeric backbones. We characterized the degradation rate, thermal stability, rheological properties, and anti-fouling capability to resist protein adsorption and cell attachment. Moreover, we further investigated the relationships between the structure and function of zwitterionic degradable polymers.

2. Experimental Section

2.1 Materials

2-Hydroxyethyl acrylate and fluorescein isothiocyanate isomer 1 were purchased from Alfa Aesar (Haverhill, MA). Methylamine (30wt% in ethanol), N-hydroxyethyl acrylamide, fetal bovine serum (FBS), polyethylene glycol (MW 200 Da) (PEG₂₀₀) diol, 100X penicillin-streptomycin solution, and bovine serum albumin (BSA) were purchased from Sigma-Aldrich (St. Louis, MO, USA). 1,6-diisocyanatohexane (HDI) and polycaprolactone (MW 2000 Da) (PCL₂₀₀₀) diol were purchased from Acros Organics (Pittsburg, PA, USA). Anhydrous dimethylformamide was obtained from EMD Millipore (Burlington, MA, USA). The cell viability/cytotoxicity assay kit was purchased from Biotium (Fremont, CA, USA). Commercial biomedical polyurethane (API-PU) materials were obtained from API (Mussolente, VI, Italy).

2.2 Synthesis of *N*-(2-hydroxyethyl)-3-(methylamino)propenamide (HMP)

First, *N*-(2-hydroxyethyl) acrylamide (9 g, 0.078 mole) was dissolved in 50 mL of ethanol. Methylamine (44 g, 1.42 mole) was then added dropwise to the solution, and the mixture was stirred overnight at 50 °C. Unreacted methylamine was removed by a rotary evaporator to yield HMP (11 g) as a colorless oil with a 96% yield. The following composition was verified by ¹H NMR (400 MHz, CDCl₃, ppm): 2.36 (s, 3H), 3.58 (t, 2H), 2.78 (t, 2H), 2.33 (t, 2H), 3.31 (q, 2H).

2.3 Synthesis of 2-hydroxyethyl 3-((3-((2-hydroxyethyl)amino)-3-oxopropyl)(methyl)amino)propanoate (CB diol)

2-hydroxyethyl acrylate (34.84 g, 0.3 mole) was added dropwise to HMP (15.23 g, 0.1 mole); the resulting solution was stirred at 0 °C for 30 minutes. Unreacted 2-hydroxyethyl acrylate was removed in a rotary evaporator. Then, the product was purified by column chromatography using ethyl acetate and methanol (10:1) as the mobile phase to yield CB diol (24.13 g) as a yellow oil with a 92% yield. The following is the composition verified by ¹H NMR (400 MHz, CDCl₃, ppm): 2.16 (s, 3H), 4.12 (t, 2H), 3.67 (t, 2H), 3.54 (t, 2H), 2.63 (t, 2H), 2.57 (t, 2H), 2.46 (t, 2H), 2.28 (t, 2H), 3.24 (q, 2H).

2.4 Synthesis of poly(carboxybetaine) degradable urethane (PCBDU)

PCBDU elastomers, which contain CB diol as a chain extender in the polymer backbone, were synthesized by two-step solvent polymerization techniques, as previously reported.⁵¹ The typical reaction was conducted in a 250 mL three-necked round bottom flask with a temperature controller, a nitrogen inlet, and a mechanical stirrer. First, PCL-diol was melted at 80 °C under nitrogen. After melting, hexamethylene diisocyanate (HDI) was added dropwise into the flask; moreover, anhydrous DMF was added to reduce the viscosity after 10-15 minutes. This prepolymer solution was stirred for two hours at 80 °C. CB diol, which depends on the feed ratio, was added to the solution dropwise, and the solution was stirred for a further 30 minutes. The resulting solution was poured into a PTFE plate, which was subsequently placed in a vacuum oven at 100 °C for 12 hours to enable the reaction to complete, and another 12 hours to remove the residual solvent under vacuum. PCBDU-1, PCBDU-3, PCBDU-5, and PCBDU-7 are elastomers with different molar ratios of HDI, PCL diol, and CB diol, i.e., 2:1:1, 4:1:3, 6:1:5, and 8:1:7, respectively. Poly(PCL-co-PEG-urethane) (PEGCU-7) with an HDI: PCL diol: PEG₂₀₀-diol ratio of 8:1:7 was synthesized and used as a control in protein adsorption and cell attachment studies. Degradable urethane (PCLDU-10) with an HDI: PCL diol ratio of 1:1 was synthesized by a similar procedure and used as a control for the degradation study. The composition of the polymers was verified by ¹H NMR (400 MHz, CDCl₃, ppm). The molecular weight and polydispersity index (PDI) were analyzed in tetrahydrofuran (THF) by size exclusion chromatography (SEC) (HPLC LC20-AD, Shimadzu, Japan) equipped with two Agilent PLgel 5μm MIXED-D columns (Agilent, Santa Clara, CA) and a Wyatt Dawn HELEOS II (Wyatt, Santa Barbara, CA) multi-angle static light scattering detector. Because of the high sensitivity of isocyanate to moisture, no isocyanate signal was detected by NMR and Fourier transform infrared spectroscopy after the reaction. All materials were also equilibrated with DI water to quench the undetectable amount of isocyanate before the characterizations.

2.5 Fourier transform infrared spectroscopy (FT-IR)

The chemical structures of the PCBDU samples at room temperature were analyzed by FT-IR using a Shimadzu IRTracer-100 Fourier transform infrared spectrometer

with a GladiATR (diamond prism) single bounce attenuated total reflection (ATR). The wavenumber ranged from 400 to 4000 cm^{-1} with 32 scans.

2.6 Differential scanning calorimetry (DSC) analysis

A Discovery DSC 2500 (TA Instrument, New Castle, DE) was used for determining the calorimetric behavior. Temperature calibration was conducted with the extrapolated onset temperature of phase transition of indium standard samples. 7 mg samples were placed on Tzero aluminum pans. The following processes were performed with a heating/cooling rate of 10 $^{\circ}\text{C}/\text{min}$ and a continuous N_2 flow of 25 mL/min. The samples were heated from 25 to 150 $^{\circ}\text{C}$ and then cooled to -90 $^{\circ}\text{C}$ to measure the cooling behavior. Subsequently, the samples were heated from -90 to +150 $^{\circ}\text{C}$ to obtain the heating curve.

2.7 Thermogravimetric analysis (TGA)

A thermogravimetric analyzer (Discovery, TA Instrument, New Castle, DE) was used to study the thermal stability of the PCBUDU materials. Here, 5 mg samples were prepared and placed on standard platinum pans. The temperature range was 50 to 700 $^{\circ}\text{C}$ with a heating rate of 10 $^{\circ}\text{C}/\text{min}$ and a continuous N_2 flow of 50 mL/min.

2.8 Compression test

The stress-strain properties of PCBUDUs were determined by a Shimadzu EZ-Test Compact Bench Testing Machine (Shimadzu Corporation, Nakagyo-Ku, Kyoto, Japan). Each sample (a disc with a diameter of 8 mm and thickness of 2 mm) was submerged in DI water for different lengths of time (0, 1, 2, and 4 h), dried, and compressed to failure at a rate of 1 mm/min with a 5000 N load cell.

2.9 Rheological study

Rheological experiments were conducted using a stress controller rotation rheometer (ARES-G2) equipped with 8 mm parallel plates with a 0.1 mm gap thickness. Strain sweep measurements were performed from 0.1% to 100% with a frequency of 10 rad/s to verify the linear viscoelastic regime. Temperature sweep studies were then carried out under the heating process from -75 $^{\circ}\text{C}$ to +100 $^{\circ}\text{C}$. The evolution of the mechanical properties was monitored by an oscillatory test at constant strain ($\gamma = 1\%$) and constant frequency ($\omega = 10$ rad/s). To ensure that the samples were completely melted, the frequency sweep tests were conducted at 100 $^{\circ}\text{C}$ under a strain of 1%. Direct

optical observations were carried out in the rheometer by a CCD camera equipped with a 5× magnification objective.

2.10 Swelling study

PCBDU samples (8 mm in diameter and 2 mm in thickness) were submerged in 5 mL DI water for two weeks to equilibrate. Then, the mass of the PU materials was recorded. Subsequently, the samples were placed in a freeze-dryer and lyophilized before being measured again. The swelling ratio (Q) was calculated using the following equation:

$$Q = \frac{M_S - M_D}{M_D} \times 100\%,$$

where M_S is the mass after swelling, and M_D is the mass after lyophilizing.

2.11 Hydrolysis kinetics pH study

Each sample with a diameter of 8 mm and a thickness of 2 mm was placed in a 20-mL vial with 5 mL of DI water at room temperature. The pH of the solution was measured and recorded by a pH meter (Mettler Toledo, USA) every 5 min for the first 30 min, and then once a day for 21 days.

2.12 Hydrolytic degradation behavior

Each sample (a disc with a diameter of 6 mm and a thickness of 1 mm) was placed individually in 20-mL vials with 2 mL of DI water and PBS at room temperature. The samples were then removed at predetermined times (2, 4, 6, 8, 10, 12, and 14 days) and dried in a vacuum oven at 85 °C overnight. The weight of the sample was then measured. The degree of degradation was determined as a weight percentage as follows:

$$\text{Weight percent} = \frac{W_t}{W_0} \times 100\%,$$

Where W_0 is the dry weight before degradation, and W_t is the dry weight at time t.

2.13 Protein adsorption study

The adsorption of protein on the PCBDU samples was studied by a fluorescent method reported previously.⁵² To evaluate the hydrolysis process of each PCBDU and API-PU/PEGCU-7 control, a sample (a disc with a diameter of 8 mm and thickness of 2 mm) of each was submerged in DI water or pH-8.5 Tris buffer for different lengths

of time (0, 1, 2, 4, 8, 12, 24, 48, and 96 h for DI water; 15, 30, 60, 90, and 120 min for pH-8.5 Tris buffer). Then, the samples were transferred into a sterile 24-well plate. Subsequently, 1 mL of FITC-labelled bovine serum albumin (FITC-BSA) solution (1 mg/mL) was added to each well. All the samples were immersed for 30 min to permit protein to adsorb on the surfaces. Following this, the samples were rinsed with PBS three times to remove loosely adsorbed proteins. The protein adsorption on a PU surface was visualized with an Olympus IX81 fluorescent microscope (Olympus, Japan), with a 40× objective lens, through a FITC filter at a fixed exposure time (200 ms) for all samples. The exposure time of the microscope was adjusted with the samples having no contact with FITC-BSA until an utterly dark background was obtained. ImageJ software was used to quantify the fluorescent intensity of each sample.

2.14 Mammalian cell attachment

Cell attachment on all PCBDU, PCLDU-10, and PEGCU-7 surfaces was studied under three different conditions. (1) Before hydrolysis and (2) After hydrolysis of PCBDU, each sample and control materials (a disc with a diameter of 8 mm and thickness of 2 mm) were submerged into 100% FBS for different lengths of time (1, 3, 7, 14 days). At each time point, samples were transferred into a sterilized 24-well plate. NIH-3T3 cells were seeded on different sample surfaces at 10^5 cells/well with 1 mL DMEM medium consisting of 10% FBS, 1% L-glutamine, and 1% penicillin-streptomycin. The samples were kept in an incubator with 5% CO₂ at 37 °C for 24 hours. Subsequently, 1 mL fresh medium was added to wash out dead cells three times, and 1 mL Calcein AM solution was added to each well. After incubation for 45 min at room temperature, Calcein AM solution was aspirated, and 1 mL fresh medium was added to remove extra dye three times. (3) Different samples were placed in a 6-well plate and submerged into the DMEM medium for three days. Then 1 mL fresh medium and 1 mL medium with 1×10^5 suspended cells were added to each well. In the following days, the old medium and dead cells were aspirated, and the cell solution containing 1×10^5 cells was added into each well every day with a fresh medium. After different timepoint (1, 3, 7, 14 days), the samples were taken out, transferred into a 24-well plate, and incubated with Calcein AM dye for 45 minutes at room temperature.

After washed out the extra dye, cell density and cell morphology were visualized with the Olympus IX81 fluorescent microscope with a 10X objective lens through FITC filters.

2.15 Statistical analysis

Protein adsorption experiments were repeated three times. Data were displayed as means \pm standard deviation. Statistical significance ($p < 0.05$) was performed using a one-way analysis of variance (ANOVA) followed by Bonferroni's post hot test.

3. Results and discussion

3.1 Synthesis of PCBDU

PCL has been used as the critical component in PU owing to its thermal plasticity, high modulus, and degradability. However, existing PCL-based PUs exhibit a few shortcomings, including a non-adjustable degradation rate, low elasticity, and insufficient anti-fouling properties. These drawbacks cause inflammation, FBR, and blood coagulation. We designed and synthesized a set of degradable PCBDUs by copolymerizing HDI, CB diol, and PCL diol at different ratios to address these challenges. The structures of the PCBDU polymers are shown in Figure 1. PCBDUs contain hydrolyzable, tertiary amine-based CB diols in the polymer backbone. The CB diol plays multiple roles in PUs by simultaneously serving as a hard segment, a chain extender, and an anti-fouling precursor. In addition, the amide bond in the CB diol is designed to improve the elasticity and hydrophilicity and further regulate the degradation process of PCBDUs. CB diol can be readily synthesized by the Michael addition reaction with a high yield in the final step.⁵³ Four PCBDUs with different stoichiometric ratios of PCL diol/CB diol, named PCBDU-1, PCBDU-3, PCBDU-5, and PCBDU-7, were synthesized via a two-step polymerization reaction. The chemical structures of CB diol and PCBDUs were verified by ¹H NMR spectroscopy (Figure S2 and S3). The increasing integrals of two signature protons (the peak at 4.24 ppm) on CB diol indicate the increasing CB diol content ratio from PCBDU-1 to PCBDU-7 samples. The NMR analysis clearly showed no DMF residue in the polymer. The molecular weight and polydispersity index (PDI) of PCBDUs and controls were analyzed by GPC. As shown in Fig S9, all PCBDUs show a narrower molecular weight distribution with a PDI below 1.25 than PCLDU-10 with a PDI of

1.48 and PEGCU-7 with a PDI of 2.09. The number average molecular weight (M_n) is 30, 26, 27, and 26 KD for PCBUDU-1, PCBUDU-3, PCBUDU-5, and PCBUDU-7, respectively. The narrow molecular weight distribution and the high M_n of PCBUDUs indicate the high conversion of the reaction and lead to the consistent properties of materials. In PCBUDU, the mechanical, anti-fouling, and degradation properties can be adjusted by tuning the PCL and CB ratio. PCBUDU can be synthesized using the standard polyurethane synthetic method and using CB diol to replace the existing polyols in the current commercially available biomedical PU formulation. No post-fabrication or surface modification is needed because the antifouling moieties are directly incorporated into the polymer backbone.

3.2 Fourier transform infrared spectroscopy (FT-IR)

PCBUDUs were characterized by FT-IR (Figure 2) to verify their compositions. The symmetric and asymmetric stretching vibrations of the C-H bond were displayed at 2933 and 2862 cm^{-1} . The sharp peaks at 1720 cm^{-1} and 1654 cm^{-1} correspond to C=O stretching vibrations and indicate the carbonyl group on the urethane and carboxyl group on PCL and CB, respectively. The absorption bands of N-H stretching vibrations were observed at 3327 cm^{-1} . FT-IR spectra showed the characteristic C-O stretching bands of both CB and PCL at 1159 cm^{-1} . Noise observed in the range of 2000–2500 cm^{-1} was due to the reflection of the diamond prism in the instrument. In all PCBUDUs, there was no signal at 2270 cm^{-1} (-NCO stretching) or 3590 cm^{-1} (O-H stretching), indicating that no isocyanate group remains in the final products. It is noteworthy that isocyanate is highly active and toxic, and it needs to be quenched or removed.

3.3 Thermal stability and thermal transition behavior

The thermal stability and transition behavior of polymeric materials are critical parameters that determine the operating conditions for fabrication and processing. The calorimetric study was performed to determine the temperature for the phase transition of PCBUDUs. As shown in Figure 3, all PCBUDUs exhibited a crystallization temperature (T_c) below -1 °C. Compared to the other three PCBUDUs, PCBUDU-1 shows a narrower crystallization peak, which is probably due to its highest PCL content among all PCBUDUs. PCL results in a narrower range of crystal dimensions and more

perfect crystals.⁵⁴ With the increase in CB content, interactions between the soft and hard segments gradually changed the crystallization structure. There was no apparent glass transition temperature (T_g) observed in the DSC profiles of all PCBUDs. It is presumably because of the kinetic-dominant crystallization process playing an essential role in heating behavior. Insufficient time was permitted to release heat from segment movement during the glass transition process before forming the crystal structure, resulting in unchanged heat-capacity. However, the glass transition process can still be monitored by more sensitive mechanical properties variation, which will be discussed further in the rheological studies. The melting temperature (T_m), which refers to the transition from a semi-crystalline to an amorphous state, is 38.8, 44.7, 44.8, and 44.8 °C for PCBUD-1, PCBUD-3, PCBUD-5, and PCBUD-7, respectively. In general, the lower the crystallization temperature, the lower the melting point of PCBUD-3, PCBUD-5, and PCBUD-7. However, the crystal dimensions, particularly the polymer microstructure, also need to be considered (PCBUD-1). It is known that the crystallinity of constituent chains is intimately related to the crystal orientation, and the crystallization mechanism in confined space mainly drives this orientation.⁵⁴ ⁵⁵ The crystallization mechanism of polymers is regulated by several factors, including size, structure, and stereoregularity of polymers chains.⁵⁶ Therefore, further studies to observe crystallization behavior and crystal orientation of PCBUDs are desired.

Figure 4 presents the TGA thermograms of PCBUDs. PCBUD-3, PCBUD-5, and PCBUD-7 exhibited two degradation stages; the first stage was 241-297 °C, 221-288 °C, and 212-283 °C, respectively. The first stage represents the degradation of the hard segment, which leads to the relatively low thermal stability of polyurethane. During the first stage of degradation, the percentages of weight loss were 19.8%, 27.4%, and 32.7% for PCBUD-3, PCBUD-5, and PCBUD-7. It clearly shows that weight loss increases as the CB diol content increases. In the second stage of degradation, the degradation temperature ranges of PCBUD-3, PCBUD-5, and PCBUD-7 were 297-375 °C, 288-386 °C, and 283-396 °C, respectively. The percentages of weight loss were 78.9%, 71.9%, and 66.7% for PCBUD-3, PCBUD-5, and PCBUD-7, respectively. In this stage, the high molecular-weight PCL soft

segments decomposed, and the weight loss in the second stage was in accord with the decrease of the PCL content in the material. Our results are consistent with other studies showing the high degradation temperatures of PCL and other polyesters, ranging from 300-400 °C.⁵⁷ In contrast to other PCBUDs, there was only one stage located at 300–358 °C for PCBUD-1. The degradation of hard segments can be barely detected in PCBUD-1 because the weight percent of CB diol in PCBUD-1 is only 10.1%. Therefore, we believed that the signal for the decomposition of the CB diol is masked. TGA study clearly shows that the decomposition temperature of PCBUDs increase as the PCL content increases. However, it should be noted that the decomposition temperatures of all PCBUDs are much higher than their melting temperature, which determines the processing temperature, even though the CB component leads to lower decomposition temperatures of PCBUDs,

3.4 Mechanical properties

Representative compressive stress-strain curves for PCBUDs under the dry condition are shown in Figure 5. The mechanical properties of the PCBUDs show a good correlation with the CB: PCL ratio. Under the dry condition, all PCBUDs remained intact at the limit stress of 25 MPa, and showed an apparent rubbery plateau, indicating chain entanglement in polymers. The rubbery plateau of PCBUDs appears at the slightly different strain ranges as PCBUD-1 < PCBUD-7 < PCBUD-5 < PCBUD-3. The strain at the high-stress region increased with the increase of the CB content. PCBUD-3 exhibited the lowest modulus at the higher strain range among all PCBUDs. It is probably due to the low interfacial strength or higher phase separation structures between the soft and hard domains in PCBUD-3, which is caused by the balanced CB: PCL ratio. Unlike PCBUD-3, the higher PCL content in PCBUD-1 leads to a more extensive continuous phase of the soft segment, and the higher CB content in PCBUD-5 and PCBUD-7 generates a larger continuous phase of the hard domain. Both the larger continuous phase and separation phase increase the modulus of the materials. It is noteworthy that the mechanical properties of PEGCU-7, which was used as the control in the protein adsorption and cell attachment studies, could not be studied because the material swelled significantly in water and was very fragile.

As expected, the compressive modulus and breaking strain of hydrated PCBDU samples were demonstrated to decrease with increasing hydrolysis time (Figure 6). All PCBDUs exhibited a high modulus, 47.9, 42.3, 41.8, and 26.1 MPa for PCBDU-1, PCBDU-3, PCBDU-5, and PCBDU-7, respectively. The compressive modulus of PCBDU-1 decreased by 11% after 1-hour hydrolysis and 81% after 24 hours. In a similar trend, the compressive modulus of PCBDU-3, PCBDU-5, and PCBDU-7 underwent a gradual decline as the hydrolysis time increased, leading to over 80% reduction after 24 hours. The modulus change is caused by the cleavage of the polymer chain via the hydrolysis of the CB diol ester and the water penetration in the polymer matrix. Even though the compressive modulus of all PCBDUs reduced after the equilibrium in water, it still behaves like a polyurethane elastomer with a modulus in the range of MPa, which is 8.9, 7.4, 6.2, and 3.5 MPa for PCBDU-1, PCBDU-3, PCBDU-5, and PCBDU-7, respectively.

3.5 Rheological study

To understand the viscoelasticity of PCBDUs under different temperatures, we measured the evolution of the storage modulus (G') and loss modulus (G'') during heating. As shown in (Figure 7), the results indicated that both G' and G'' were susceptible to structural alterations in PCBDUs. Moreover, in the low-temperature range (< -40 °C), G' is greater than G'' , because polymers are in the glassy region, and the polymer chains are stiff and rigid. As the temperature increased, the storage modulus and loss modulus of PCBDUs underwent a marginal reduction (glass transition region) and then reached a plateau (rubbery plateau region), which indicates the transition from glassy material to soft rubber. At high temperatures (> 20 °C), both storage modulus and loss modulus decreased remarkably, indicating a melting transition. After a crossover of G' and G'' , the polymers became a viscoelastic liquid.

Frequency sweep experiments at 100 °C were performed to verify the liquid-like behavior of PCBDUs. As shown in Figure 8, all the PCBDUs demonstrated an increasing modulus and a decreasing viscosity with the increase of the frequency, which corresponds to the behavior of liquid-like materials. At the high-frequency range (100 to 1 rad/s), all PCBDUs exhibited higher G'' than G' . However, in the low-

frequency regime (10^{-1} - 10^0 rad/s), both PCBDU-3 and PCBDU-5 displayed a crossover of G' and G'' . Moreover, the G' of PCBDU-7 showed higher fluctuation, which might be caused by the crystal microstructure or the stronger intermolecular hydrogen bonding interactions.

During the heating process, two transition temperatures were obtained (Table 1). The glass transition temperature of PCBUDs increase with the increase of the CB diol content, which leads to higher hard segment content. Meanwhile, the melting temperature did not exhibit noticeable differences among PCBUDs. The melting temperatures obtained in the rheological study were marginally higher than those obtained in the DSC measurements. It is presumably because the crystal structure (kinetic-dominant process) exerts a more significant effect on the mechanical properties than heat capacities. An advantage of PCBUDs is their significantly lower melting temperatures compared to quaternary ammonium-based zwitterionic PUs.⁵⁸ The latter requires over 250 °C of processing temperature for extrusion or injection molding, and the melting temperature is close to the material decomposition temperature.

3.6 Water absorption, hydrolysis kinetics, and degradation studies

Because the water content of polymeric materials determines their mechanical, hydrolysis kinetics, and swelling properties, the water uptake and weight loss of PCBUDs as a function of time were measured. As shown in Table 1, the swelling ratios of PCBUDs increased with the increase of the CB content. After two weeks, the weight percent of the absorbed water ranged from 13.0% for PCBDU-1 to 52.2% for PCBDU-7. The swelling behavior of the degradable polymers is determined by the change of porosity and hydrophilicity of the material caused by the hydrolysis of the polymer backbone. PCBUDs contain urethane bonds, amide bonds, regular ester bonds, and beta-amino ester bonds along their polymer backbone. Among these bonds, both regular ester bonds and beta-amino ester are more susceptible to hydrolysis; beta-amino ester bonds undergo much faster hydrolysis than the typical esters.⁵⁹ The hydrolysis of the ester bonds of the CB diols in the backbone generates charged anions and cations, leading to water adsorption. The breakage of the polymer chains also results in the formation of channels for water penetration. Because the CB diol

contains polar amide and tertiary amine groups, the CB segment is more hydrophilic than the PCL segment, and therefore the higher CB content results in higher water uptake. In addition, the urethane group makes a significant contribution to the water uptake of the material. Each diol forms two urethane bonds at the end. Because the CB diol has a much lower molecular weight than the PCL diol, the hard segments of PCBDUs carry much higher urethane bond density than the soft segments. Furthermore, the more organized crystal structure in PCBDU with the higher PCL content also minimized water penetration. So, in this material platform, multiple physical and chemical parameters can be used to tune and control water adsorption. In addition to the faster hydrolysis of the beta-amine ester than the regular ester, PCBDUs also carry a self-catalyzed hydrolysis property in DI water. The protonation of tertiary amine groups in the CB segment generates hydroxides and leads to a high pH after the material is submerged in DI water. The resulting hydroxides cause the hydrolysis of the ester bonds. The hydrolysis of the ester groups consumes hydroxide and decreases the pH of the solution. The pH of the solution eventually becomes stable when the equilibrium in the hydrolysis of esters is reached. As shown in Figure S8, all the solutions were basic initially, and the pH value of the solution for all PCBDUs decreased gradually. At the initial stage, the quick pH change from basic to neutral is caused by the faster hydrolysis of beta-amino esters in CB groups at the interface. Then all PCBDUs experience a short plateau period between pH 6-7. We believe it is caused by the buffering effect of the tertiary amine group in CB. Because the hydrolysis of the ester bond in PCL continues to generate acids, the pH continues to drop until it reaches equilibrium. At the end of the study, PCBDUs with a higher CB content exhibited a slightly lower pH. The lower pKa value of carboxylate was caused by the pK_b of the tertiary amine in beta-amino ester.³⁶ The pH profiles in the hydrolysis study indicate that the CB content of PCBDUs determines the hydrolysis kinetics and significantly affects the swelling properties and the degradation rate. The anti-fouling property of the materials requires the zwitterionic carboxybetaine that is generated by the hydrolysis of the beta-amino ester in the CB diol. The rapid hydrolysis of beta-amino ester in DI water avoids the long post-fabrication processing time and the use of a strong base. Because of its significantly higher polarity, we

hypothesized that zwitterionic carboxybetaine groups enrich at the water–material interface; however, further study is needed to validate the theory.

The degradation kinetics of PCBUDs in DI water and PBS was also measured. Figure 9 shows the decrease in weight of all PCBUDs during the hydrolysis. PCLDU-10, which contains 100% PCL as the diol, was used as a control material. After 14 days, the PCLDU-10 exhibited 94.8% and 94.2% of its original weight in water and PBS, whereas the weight percentages of the PCBUD samples ranged from 94.4% to 58.0% in water and from 94.9% to 58.7% in PBS as the CB content increases. The faster hydrolysis of beta-amine ester in the CB diol than the regular ester in PCL causes the faster weight loss of PCBUDs with the higher CB content. This study demonstrated that the degradation rate of PCBUD could be finely tuned by adjusting the ratio of CB diol and the structure of the polymer. Our results also agree with previous studies in that the beta-amino ester group⁵⁹ hydrolyzes significantly faster than the regular ester bond. It is worth noting that the degradation products of the CB component are alcohol and tertiary amine-based zwitterionic carboxybetaine, which would not lead to a dramatic pH change in the solution. It is well known that the hydrolysis of the polyesters, including polylactide and PCL, generate acid and lead to a local pH drop, which may cause inflammation.⁶⁰ Our previous study demonstrated that the tertiary amine in CB diol has a buffer capacity between pH 6.5-8.5³⁶. We also observed the buffering effect of zwitterionic CB in the hydrolysis study (Figure S8). We believe the buffer capacity of PCBUD will be beneficial for the applications, such as wound healing or tissue engineering scaffolding, which desire stable weak acidic and neutral pH. This study confirmed that beta-amino ester could be combined with regular polyesters with a lower hydrolysis rate to tune the water penetration and degradation rate of the materials, and it could also function as the buffering group to maintain a stable local pH.

3.7 Protein adsorption and mammalian cell attachment

Many studies have unveiled that material-associated thrombosis,⁶¹ biofilm formation, infection,⁶² and FBR⁴ are all initiated from the adsorption of biomolecules. To address these complications, many pioneers proposed to use anti-fouling materials to resist the adsorption of biomacromolecules. We expect that the highly polar CB

moieties would be enriched at the water/material interface, whereas the hydrophobic PCL domains tended to minimize the interaction with water. The hydrolysis of the beta-amino ester bond will rapidly generate zwitterionic CB anti-fouling groups at the surface. To test our hypothesis, we used FITC-labeled BSA as the model protein to evaluate the anti-fouling properties of PCBUDs. The ratio of fluorescence intensities between each sample and API-PU positive control were calculated and are shown in Figure 10. It was found that the protein adsorption on all PCBUDs decreased as a function of hydrolysis time. PCBUD-3 exhibited relatively higher protein adsorption compared to other PCBUDs at the initial stage. However, it eventually reaches the same level as other PCBUDs. It is possible because there were not enough CB groups on the surface of PCBUD-3 due to its different microstructure than PCBUD-5 and PCBUD-7. The higher hydrophobic PCL content on the material surface leads to protein adsorption. The higher CB: PCL ratio in PCBUD-5 and PCBUD-7 lead to the quick generation of anti-fouling properties. After 24 hours in DI water and two hours in pH 8.5 Tris buffer, all the PCBUD surfaces reached 2–3% protein adsorption, which indicates that the zwitterionic carboxybetaine groups are very effective at resisting non-specific protein adsorption. We also synthesized PEG-based PU (PEGCU-7) as the positive anti-fouling control because PEG has been widely used as a gold standard anti-fouling material for protein adsorption studies. PEGCU-7 exhibited at least 40% protein adsorption under all conditions compared to API-PU, which is significantly higher than almost all PCBUDs (except PCBUD-3) even before hydrolysis. Several studies have reported that hydration and steric hindrance are critical factors for material to resist protein adsorption.⁶³ Zwitterionic materials can tightly bind water molecules via ionic solvation to form a strong hydration layer to repel proteins. The protein adsorption study further demonstrated the effectiveness of the carboxybetaine functional group over PEG to resist non-specific protein adsorption. It should be noted that one CB diol contains one carboxybetaine functional group, whereas PEG requires multiple ethylene glycol repeating units to perform the anti-fouling function. Many earlier studies discovered that extracellular matrix proteins mediate mammalian cell attachment to a surface.⁶⁴ It has been widely observed in numerous

in vitro studies that anti-fouling materials, including PEG⁶⁵ and zwitterionic polymers,⁶⁶ can reduce cell attachment due to their ability to resist non-specific protein adsorption. In the standard mammalian cell attachment studies, adherent cells are incubated with materials in the medium with 10% or less FBS for 1 to 2 days. If the adherent cells cannot firmly attach to the surface in a few hours, cells quickly die. The dead cells are no longer able to attach to the surface; even the necessary amount of proteins eventually adsorb on the surface afterward. However, the materials are always in contact with blood or extracellular fluid under *in vivo* environments. Thus, the commonly-used cell attachment procedure is not challenging enough to assess the critical anti-fouling properties of the material for *in vivo* application and may lead to false anti-fouling conclusions. To mimic the *in vivo* condition, we designed and performed three different cell attachment experiments to confirm the effectiveness of PCBUDs to resist cell attachment in the complex environment for long-term.

In the first study, we first treat PCBUDs and control materials in pH 8.5 buffer for 2 hours and incubate PCBUDs and control materials in 100% FBS for 1, 3, 7, and 14 days. Then we measured the cell attachment of NIH-3T3 fibroblast cells in DMEM medium with 10% FBS for 24 hours. The cell attachment on the PCBUD and control surfaces was measured by the fluorescent microscope (Figure S11), and the cell densities were recorded in Table S2. Under all conditions, PCLDU-10 shows the highest cell density. The cell densities increase with the increase of the incubation time in FBS. The PCLDU-10 samples, which were incubated in FBS for 14 days, were fully covered by NIH-3T3 cells. All PCBUDs highly resisted cell attachment, and almost no cell adhere to any PCBUDs that had contact with 100% FBS for 14 days. Anti-fouling PEGCU-7 control surfaces showed reduced cell attachment if they were incubated in 100% FBS for 1 and 3 days before the cell attachment study compared to PCLDU-10; however, it was fully covered by cells if it was incubated in 100% FBS for 7 days or more.

In the second study, we investigated if PCBUDs need to be treated in DI water or pH 8.5 buffer to generate zwitterionic anti-fouling CB groups before they were incubated with FBS. If the hydrolysis of PCBUDs is unnecessary, it will simplify the

manufacturing process and reduce the processing time. Unhydrolyzed PCBDUs and control materials were immersed in 100% FBS for 1, 3, 7, and 14 days. Then all materials were incubated with NIH-3T3 in a medium with 10% FBS for 24 hours. Cell densities were measured and recorded in Figure S12 and Table S3. The positive control, PCLDU-10, shows the highest cell density among all samples with the same incubation time with FBS. A small number of cells were observed on all PCBDUs that were incubated with 100% FBS for 1 day. The initial cell attachment on PCBDUs is due to the positive surface charge caused by the protonation of tertiary amines in CB diol before the complete hydrolysis. However, no cells were observed on PCBDU surfaces incubated with 100% FBS for three days. Anti-fouling PEGCU-7 control surfaces showed no cell attachment after the incubation in 100% FBS for 1 day; however, PEGCU-7 samples were covered by cells if they incubated in FBS for 7 days. It indicated that the generation of the highly potent anti-fouling CB group on the surface in FBS happened within three days. This study demonstrated that PCBDUs could be directly used without hydrolysis.

In the third study, we developed a more challenging method to mimic the *in vivo* condition wherein an implanted material is always exposed to biomacromolecules and cells. In this method, PCBDUs before the hydrolysis and control materials were incubated in DMEM medium with 10% FBS for three days to let protein adsorb on the material surfaces, and then samples were incubated with NIH-3T3 cell in DMEM medium with 10% FBS for up to 14 days. The fresh medium with new NIH-3T3 cells was used to replace the old medium every day. In this procedure, the materials are constantly challenged by new cells in the complex medium. After 1, 3, 7, and 14 days, cell densities on each sample were measured and recorded in Figure 11 and Table S4. The conventional degradable PCLDU-10 surfaces were almost entirely covered by cells after one day. Nearly half of the PEGCU-7 surface was covered by cells after three days and fully covered by the cells after seven days. As we expected, almost no cell was observed on all PCBDU surfaces under this most challenging *in vitro* condition. These studies clearly show that even PCBDU-1 with 10.1 wt% CB component is highly effective at resisting mammalian cell adhesion because of the self-replenishing of zwitterionic carboxybetaine at the interface.

Earlier studies illustrated that ultra-low fouling materials could delay blood coagulation by reducing the fibrinogen adsorption in the short term.^{67, 68} Our study clearly shows that existing anti-fouling materials do not carry the critical anti-fouling properties to resist protein adsorption from the complex protein solutions and cell attachment under the more challenging procedure, even though they can resist protein in short-term. It explained why these materials still trigger FBR and platelet activation in the body. It should be noted that PEG has been combined with various materials by both academia and industry. This study, along with previous studies,⁵¹ consistently observed that the anti-fouling property of PEG is far below the threshold needed to keep a surface clean in complex systems or *in vivo* conditions for both long-term and short-term applications.^{67, 68} New materials with a critical anti-fouling property and other tunable properties are essential for developing new therapeutic methods and biosensing technologies; however, due to the intrinsic flaws, existing materials are unlikely to solve these long-standing challenges. Recent studies have shown that different cell types displayed different adhesion behavior on polymer surfaces.⁶⁹ Therefore, the anti-cell attachment property of PCBUDs against the specific cell type needs to be evaluated for each unique application. Due to their excellent antifouling property, tunable physical properties and degradability, simplicity of fabrication, thermoplasticity, and low cost, PCBUDs are easily adapted to a wide range of biomedical and industrial applications, such as vascular graft, bioabsorbable stent, Bone grafting, drug delivery carrier, degradable biosensor, coating, etc.

Conclusion

In this work, a set of novel thermoplastic polyurethane materials with controllable degradability, superior anti-fouling property, and mechanical properties were developed via the simple and straightforward condensation polymerization method. The incorporation of degradable CB diol increases the elasticity and degradation rate of PCL. The thermal stability of PU slightly affected by introducing the CB component, and thermal transition behavior revealed the thermoplastic properties of PCBDU. Both surface and bulk hydrolysis were monitored by protein adsorption and pH kinetics. After 48 hours in water and 2 hours in pH 8.5 buffer, all samples switched to effective anti-fouling surfaces with strong resistance to non-specific protein adsorption. PCBDUs also display the unseen ability to resist cell attachment. To the best of our knowledge, there have not been any other biodegradable polymers that can resist cell adhesions for 14 days. This study provides us a deeper understanding of structure-function relationships of zwitterionic polyurethanes. The thermoplasticity will minimize the significant changes in processing and manufacturing. Our study also demonstrated the effectiveness of the strategy by tuning the molecular structure of the monomer to improve the physical and chemical properties of the polymer. This novel degradable material platform can be applied for a broad range of applications, including coating, films, or various implantable biomedical devices, which have been troubled by the long-standing material-induced thrombosis, implant-associated infections, and foreign body response.

Acknowledgments

This work was supported by the US National Science Foundation (DMR-1454837 and 1741935). Parts of this work were conducted using the Soft Matter Characterization Facility at the University of Chicago. The authors wish to thank Dr. Philip Griffin for his aid with a few experiments and the data analysis.

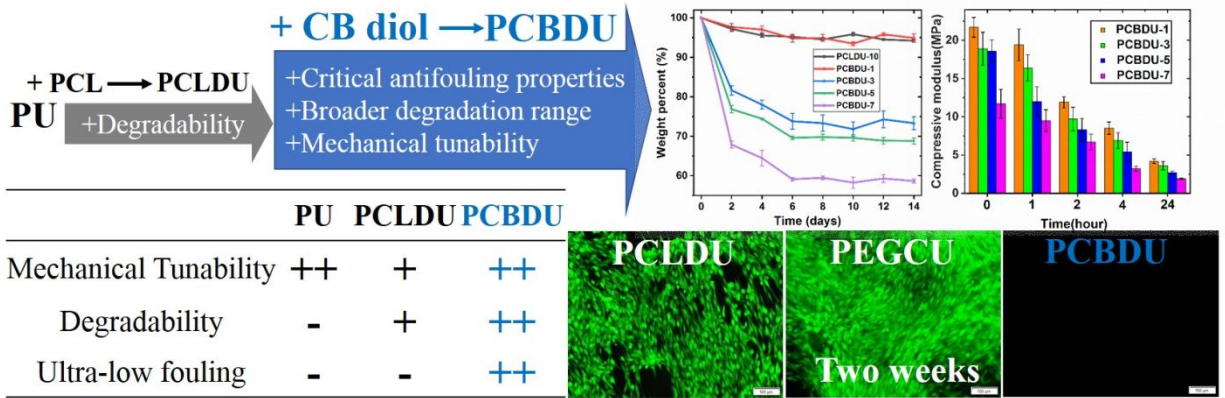
References

1. I. H. Jaffer, J. C. Fredenburgh, J. Hirsh and J. I. Weitz, *J. Thrombo. Haemost.*, 2015, **13**, S72-S81.
2. I. Francolini and G. Donelli, *FEMS Immunol. Med. Microbiol.*, 2010, **59**, 227-238.
3. S. Jiang and Z. Cao, *Adv. Mater.*, 2010, **22**, 920-932.
4. J. M. Anderson, A. Rodriguez and D. T. Chang, *Semin Immunol*, 2008, **20**, 86-100.
5. Y. Chandorkar, R. K and B. Basu, *ACS Biomater. Sci. Eng.*, 2019, **5**, 19-44.
6. B. Cao, Q. Tang and G. Cheng, *J. Biomater. Sci., Poly. Ed.*, 2014, **25**, 1502-1513.
7. S. Liu and W. Guo, *Adv. Funct. Mater.*, 2018, **28**, 1800596.
8. M. Labet and W. Thielemans, *Chem. Soc. Rev.*, 2009, **38**, 3484-3504.
9. A. J. R. Lasprilla, G. A. R. Martinez, B. H. Lunelli, A. L. Jardini and R. M. Filho, *Biotechnol. Adv.*, 2012, **30**, 321-328.
10. R. Mehta, V. Kumar, H. Bhunia and S. N. Upadhyay, *J. Macromol. Sci. Polymer Rev.*, 2005, **45**, 325-349.
11. A. Roointan, S. Kianpour, F. Memari, M. Gandomani, S. M. Gheibi Hayat and S. Mohammadi-Samani, *Int. J. Polym. Mater.*, 2018, **67**, 1028-1049.
12. L. Erdmann and K. E. Uhrich, *Biomaterials*, 2000, **21**, 1941-1946.
13. S. A. Guelcher, *Tissue Eng. Part B Rev.*, 2008, **14**, 3-17.
14. M. Sobczak, *Polym. Plast. Technol. Eng.*, 2015, **54**, 155-172.
15. S.-Y. Lee, S.-C. Wu, H. Chen, L.-L. Tsai, J.-J. Tzeng, C.-H. Lin and Y.-M. Lin, *Biomed. Res. Int.*, 2018, **2018**, 3240571-3240571.
16. C. Xu, Y. Huang, G. Yepez, Z. Wei, F. Liu, A. Bugarin, L. Tang and Y. Hong, *Scientific Reports*, 2016, **6**, 34451.
17. A. S. Xue, J. C. Koshy, W. M. Weathers, E. M. Wolfswinkel, Y. Kaufman, S. E. Sharabi, R. H. Brown, M. J. Hicks and L. H. Hollier, Jr., *Cranio-maxillofac. Trauma Reconstr.*, 2014, **7**, 27-34.
18. E. Dondossola, B. M. Holzapfel, S. Alexander, S. Filippini, D. W. Hutmacher and P. Friedl, *Nat. Biomed. Eng.*, 2016, **1**, 0007.
19. O. M. BÖSTMAN and H. K. PIHLAJAMÄKI, *J. Bone Joint Surg.*, 1998, **80**, 1791-1794.
20. C. Flege, F. Vogt, S. Höges, L. Jauer, M. Borinski, V. A. Schulte, R. Hoffmann, R. Poprawe, W. Meiners, M. Jobmann, K. Wissenbach and R. Blindt, *J. Mater. Sci. Mater. Med.*, 2013, **24**, 241-255.
21. L. Gevaux, M. Lejars, A. Margailan, J.-F. Briand, R. Bunet and C. Bressy, *Polymers*, 2019, **11**, 305.
22. J. O. Akindoyo, M. D. H. Beg, S. Ghazali, M. R. Islam, N. Jeyaratnam and A. R. Yuvaraj, *RSC Adv.*, 2016, **6**, 114453-114482.
23. R. J. Zdrahala and I. J. Zdrahala, *J. Biomater. Appl.*, 1999, **14**, 67-90.
24. A. Burke and N. Hasirci, *Biomaterials*, Boston, MA, 2004, 83-101.
25. J. W. Costerton, P. S. Stewart and E. P. Greenberg, *Science*, 1999, **284**, 1318-1322.
26. M. Sgarioto, R. Adhikari, P. A. Gunatillake, T. Moore, J. Patterson, M.-D. Nagel and F. Malherbe, *Front. Bioeng. Biotechnol.*, 2015, **3**.

27. V. Jakobi, J. Schwarze, J. A. Finlay, K. A. Nolte, S. Spöllmann, H.-W. Becker, A. S. Clare and A. Rosenhahn, *Biomacromolecules*, 2018, **19**, 402-408.
28. C. Zhao, L. Y. Li, Q. M. Wang, Q. M. Yu and J. Zheng, *Langmuir*, 2011, **27**, 4906-4913.
29. D. Leckband, S. Sheth and A. Halperin, *J. Biomater. Sci. Polym. Ed.*, 1999, **10**, 1125-1147.
30. P. K. Thalla, A. Contreras-García, H. Fadlallah, J. Barrette, G. De Crescenzo, Y. Merhi and S. Lerouge, *Biomed. Res. Int.*, 2013, **2013**, 962376-962376.
31. J. Ladd, Z. Zhang, S. Chen, J. C. Hower and S. Jiang, *Biomacromolecules*, 2008, **9**, 1357-1361.
32. M. D. Swartzlander, C. A. Barnes, A. K. Blakney, J. L. Kaar, T. R. Kyriakides and S. J. Bryant, *Biomaterials*, 2015, **41**, 26-36.
33. A. D. Lynn, T. R. Kyriakides and S. J. Bryant, *J. Biomed. Mater. Res. A*, 2010, **93A**, 941-953.
34. X. Wang, T. Ishida and H. Kiwada, *J. Control. Release*, 2007, **119**, 236-244.
35. Y.-C. Hsieh, H.-E. Wang, W.-W. Lin, S. R. Roffler, T.-C. Cheng, Y.-C. Su, J.-J. Li, C.-C. Chen, C.-H. Huang, B.-M. Chen, J.-Y. Wang, T.-L. Cheng and F.-M. Chen, *Theranostics*, 2018, **8**, 3164-3175.
36. C.-J. Lee, H. Wu, Q. Tang, B. Cao, H. Wang, H. Cong, J. Zhe, F. Xu and G. Cheng, *Langmuir*, 2015, **31**, 9965-9972.
37. H. Wang, H. Wu, C.-J. Lee, X. Lei, J. Zhe, F. Xu, F. Cheng and G. Cheng, *Langmuir*, 2016, **32**, 6544-6550.
38. B. Cao, C.-J. Lee, Z. Zeng, F. Cheng, F. Xu, H. Cong and G. Cheng, *Chem. Sci.*, 2016, **7**, 1976-1981.
39. C.-J. Lee, H. Wang, M. Young, S. Li, F. Cheng, H. Cong and G. Cheng, *Acta Biomater.*, 2018, **75**, 161-170.
40. S. Chen, J. Zheng, L. Li and S. Jiang, *J. Am. Chem. Soc.*, 2005, **127**, 14473-14478.
41. G. Cheng, Z. Zhang, S. F. Chen, J. D. Bryers and S. Y. Jiang, *Biomaterials*, 2007, **28**, 4192-4199.
42. L. Carr, G. Cheng, H. Xue and S. Jiang, *Langmuir*, 2010, **26**, 14793-14798.
43. Y. He, H.-K. Tsao and S. Jiang, *J. Phys. Chem. B*, 2012, **116**, 5766-5770.
44. B. Cao, Q. Tang, L. Li, J. Humble, H. Wu, L. Liu and G. Cheng, *Adv. Healthc. Mater.*, 2013, **2**, 1096-1102.
45. H. C. Hung, P. Jain, P. Zhang, F. Sun, A. Sinclair, T. Bai, B. W. Li, K. Wu, C. Tsao, E. J. Liu, H. S. Sundaram, X. J. Lin, P. Farahani, T. Fujihara and S. Y. Jiang, *Adv. Mater.*, 2017, **29**, 1700617.
46. H. Wang, D. E. Christiansen, S. Mehraeen and G. Cheng, *Chem. Sci.*, 2020, **11**, 4709-4721.
47. H. F. Wang, Y. Hu, D. Lynch, M. G. Young, S. X. Li, H. B. Cong, F. J. Xu and G. Cheng, *ACS Appl. Mater. Interfaces* 2018, **10**, 37609-37617.
48. S.-H. Ye, Y. Hong, H. Sakaguchi, V. Shankarraman, S.K. Luketich, A. D'Amore, W.R. Wagner, *ACS Appl. Mater. Interfaces* 2014, **6**, 22796-22806.
49. Y. Hong, S.-H. Ye, A. Nieponice, L. Soletti, D. A. Vorp and W. R. Wagner, *Biomaterials*, 2009, **30**, 2457-2467.

50. Y. Hong, S.-H. Ye, A. L. Pelinescu and W. R. Wagner, *Biomacromolecules*, 2012, **13**, 3686-3694.
51. H. Wang, Y. Hu, D. Lynch, M. Young, S. Li, H. Cong, F.-J. Xu and G. Cheng, *ACS Appl. Mater. Interfaces*, 2018, **10**, 37609-37617.
52. B. Cao, L. Li, H. Wu, Q. Tang, B. Sun, H. Dong, J. Zhe and G. Cheng, *Chem. Commun.*, 2014, **50**, 3234-3237.
53. D. P. Nair, M. Podgórski, S. Chatani, T. Gong, W. Xi, C. R. Fenoli and C. N. Bowman, *Chem. Mater.*, 2014, **26**, 724-744.
54. S. Nakagawa, K.-i. Kadena, T. Ishizone, S. Nojima, T. Shimizu, K. Yamaguchi and S. Nakahama, *Macromolecules*, 2012, **45**, 1892-1900.
55. T.-M. Chung, T.-C. Wang, R.-M. Ho, Y.-S. Sun and B.-T. Ko, *Macromolecules*, 2010, **43**, 6237-6240.
56. D. Mileva, D. Tranchida and M. Gahleitner, *Polym. Crystallization*, 2018, **1**, e10009.
57. S. Gautam, C.-F. Chou, A. Dinda, D. P. Potdar and N. Mishra, *J. Mater. Sci.*, 2014, **49**.
58. P. N. Coneski and J. H. Wynne, *ACS Appl. Mater. Interfaces*, 2012, **4**, 4465-4469.
59. D. M. Lynn and R. Langer, *J. Am. Chem. Soc.*, 2000, **122**, 10761-10768.
60. D. Wu, X. Chen, T. Chen, C. Ding, W. Wu and J. Li, *Sci. Rep.*, 2015, **5**, 11105.
61. I. H. Jaffer, J. C. Fredenburgh, J. Hirsh and J. I. Weitz, *J. Thromb. Haemost.*, 2015, **13**, S72-S81.
62. C. R. Arciola, F. I. Alvi, Y. H. An, D. Campoccia and L. Montanaro, *Int. J. Artif. Organs.*, 2005, **28**, 1119-1125.
63. M. He, K. Gao, L. Zhou, Z. Jiao, M. Wu, J. Cao, X. You, Z. Cai, Y. Su and Z. Jiang, *Acta Biomater.*, 2016, **40**, 142-152.
64. L. Stavalone and V. Lionetti, *Front. Microbiol.*, 2017, **8**, 1760.
65. P. D. Drumheller and J. A. Hubbell, *J. Biomed. Mater. Res.*, 1995, **29**, 207-215.
66. B. Cao, L. Li, Q. Tang and G. Cheng, *Biomaterials*, 2013, **34**, 7592-7600.
67. W.-B. Tsai, J. M. Grunkemeier and T. A. Horbett, *J. Biomed. Mater. Res.*, 1999, **44**, 130-139.
68. M. Shen, L. Martinson, M. Wagner, D. Castner, B. Ratner and T. Horbett, *J. Biomater. Sci. Polym. Ed.*, 2002, **13**, 367-390.
69. J. Lian, H. Xu, S. Duan, X. Ding, Y. Hu, N. Zhao, X. Ding, F.-J. Xu, *Biomacromolecules* 21 (2020) 732-742.

TOC



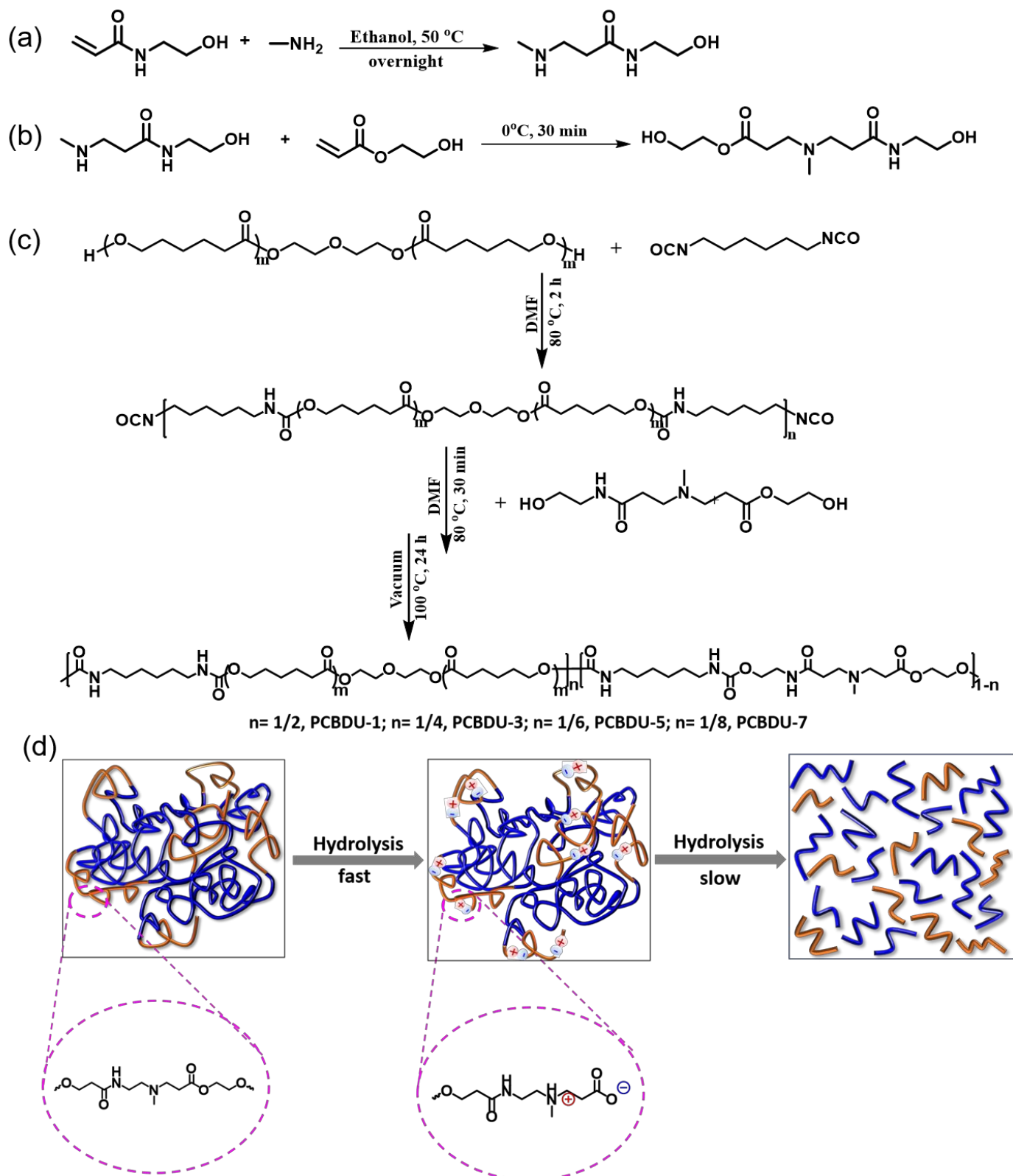


Figure 1. Synthetic route of (a) HMP, (b) CB-diol and (c) PCBDU polymers. (d) Schematic illustration of the hydrolysis process of PCBDU polymers.

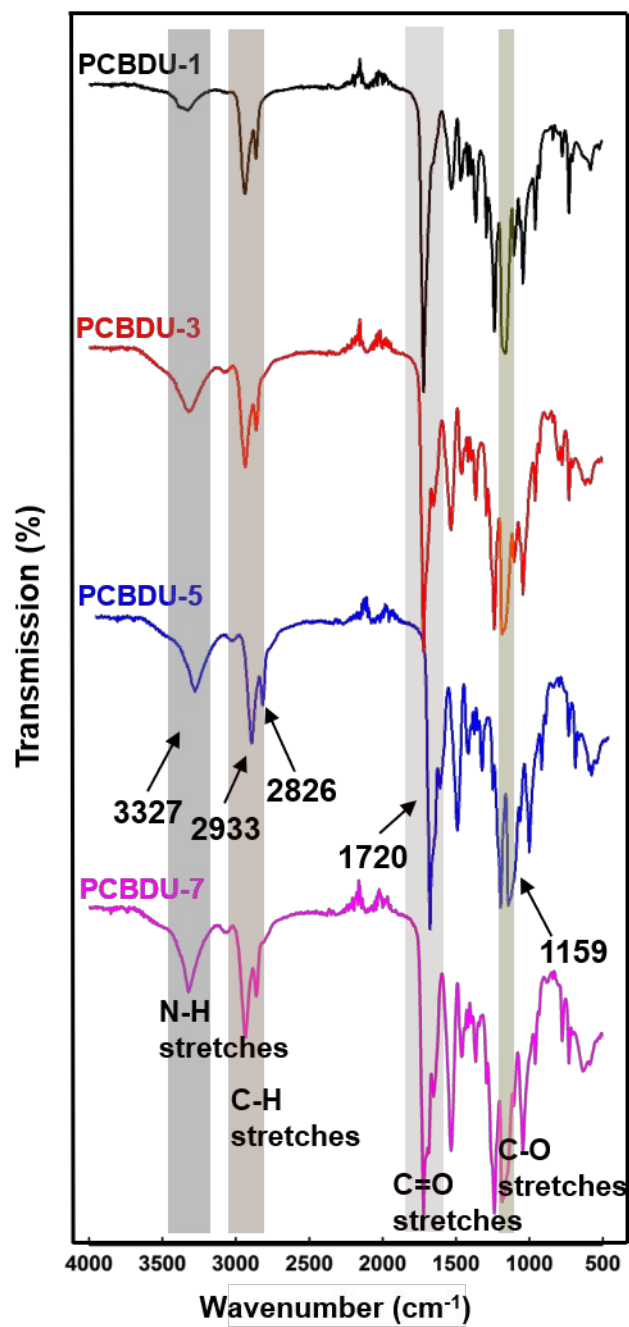


Figure 2. FT-IR spectrum for PCBDU polymers.

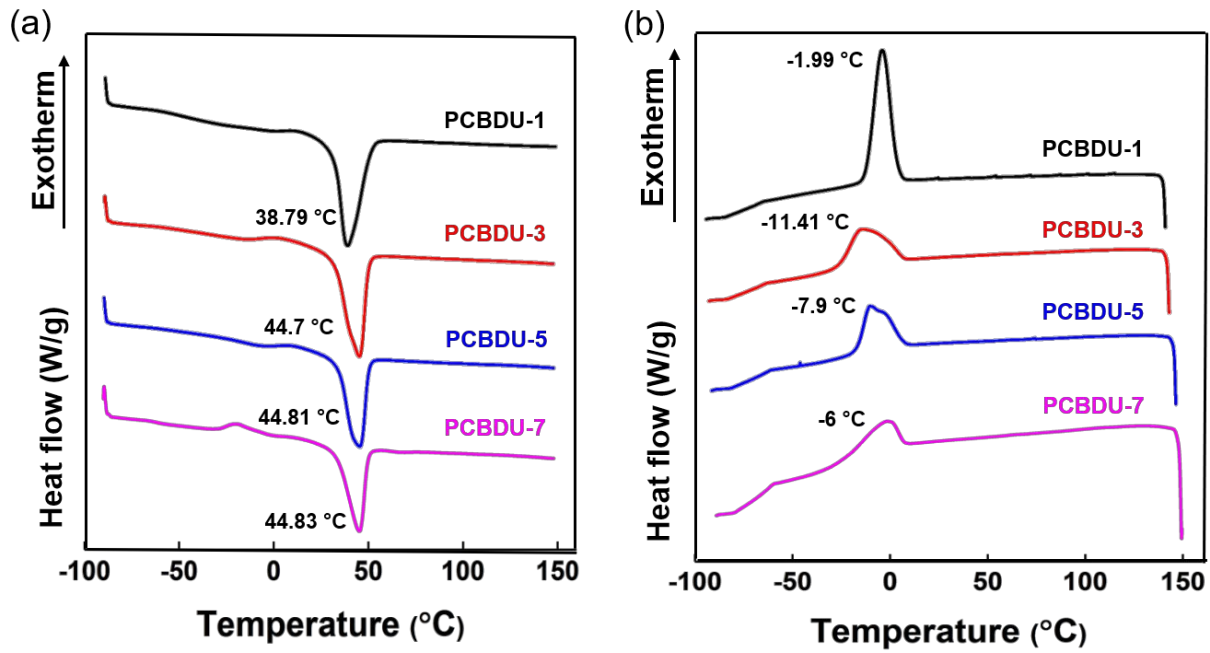


Figure 3. DSC profile of (a) heating curve and (b) cooling curve of PCBDU polymers.

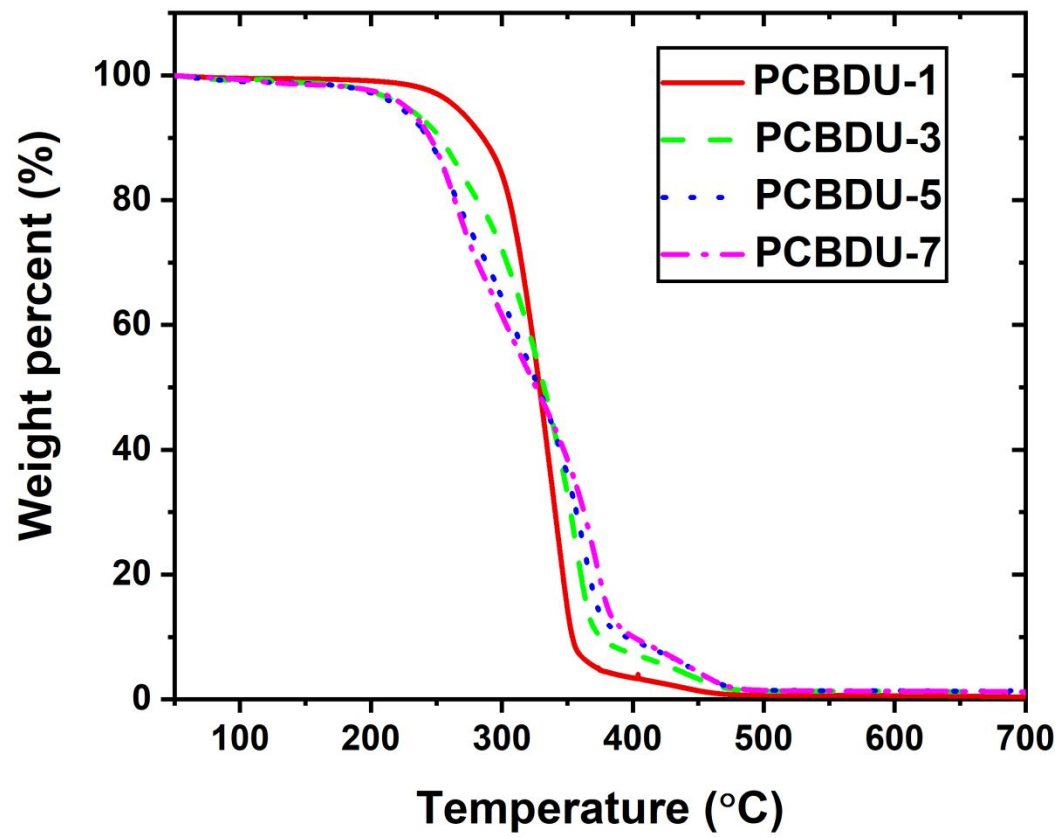


Figure 4. TGA profile of PCBUDU polymers.

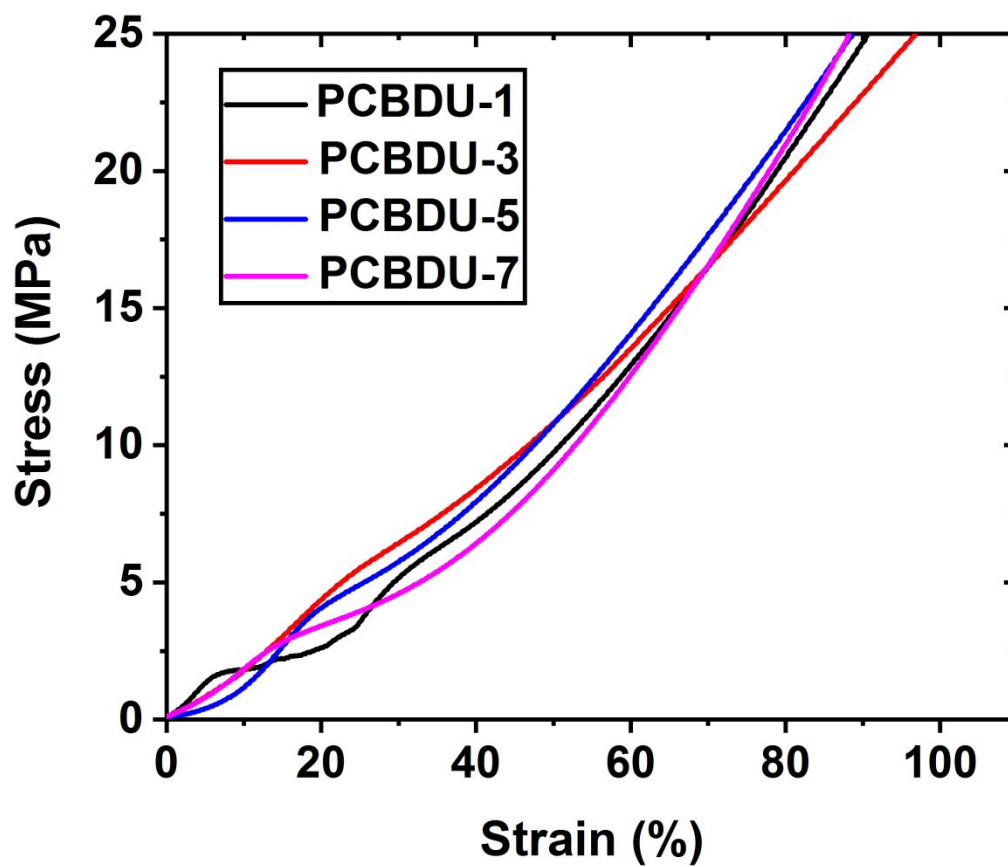


Figure 5. Stress-strain curve of PCBDU polymers under dry condition.

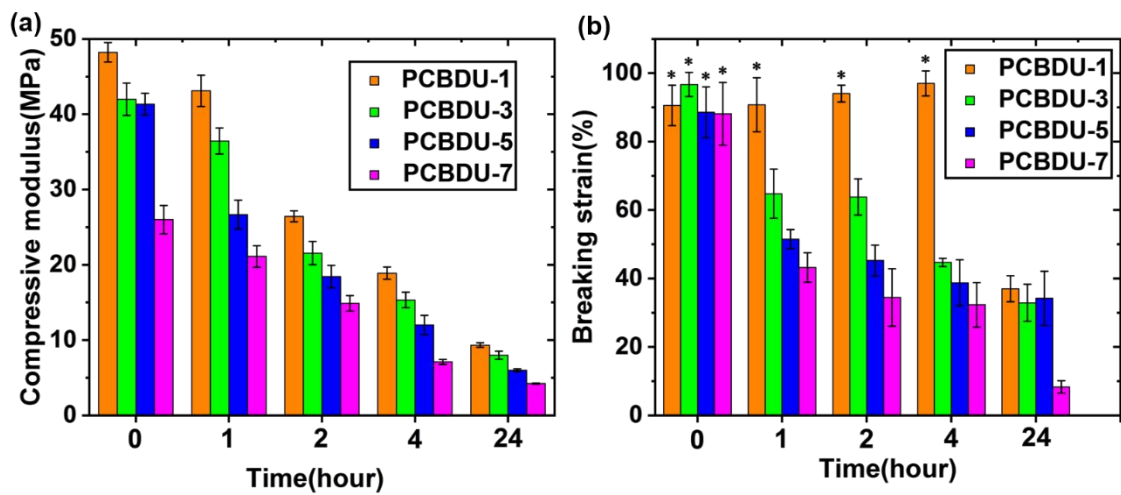


Figure 6. (a) Compressive modulus and (b) breaking strain of PCBDU polymers under the wet condition with different hydrolysis times. * means that the sample did not break when the compression stress reached the limit of 5000N.

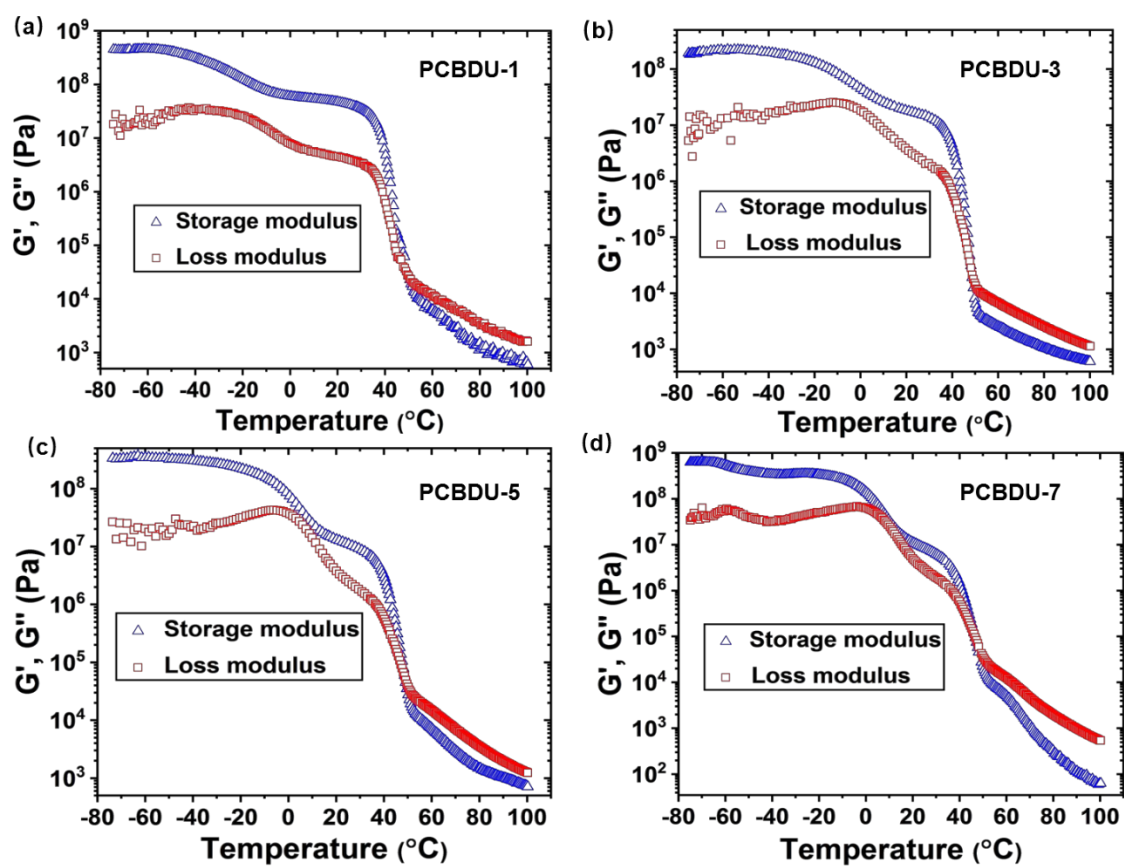


Figure 7. Temperature sweep rheological studies of (a) PCBDU-1, (b) PCBDU-3, (c) PCBDU-5, and (d) PCBDU-7.

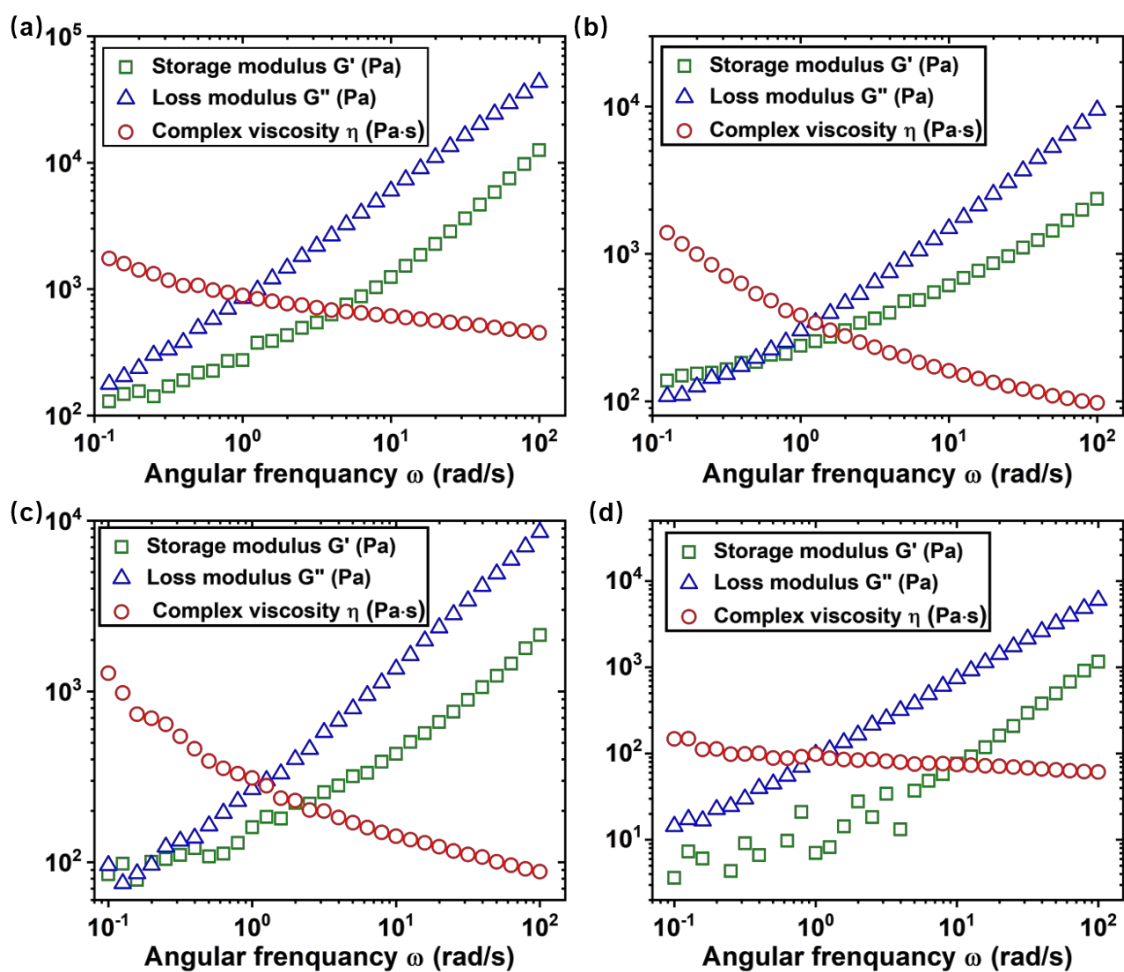


Figure 8. Frequency sweep rheological studies of (a) PCBDU-1, (b) PCBDU-3, (c) PCBDU-5, and (d) PCBDU-7.

Table 1. Glass transition temperature and melting temperature of PCBDUs obtained from the rheology study and swelling ratio of PCBDUs after two weeks of immersion in water.

	T_g (°C)	T_m (°C)	Swelling ratio Q (%)
PCBDU-1	-38.8	50.0	13.0
PCBDU-3	-26.0	48.4	25.3
PCBDU-5	-14.8	48.8	37.0
PCBDU-7	4.3	46.6	52.2

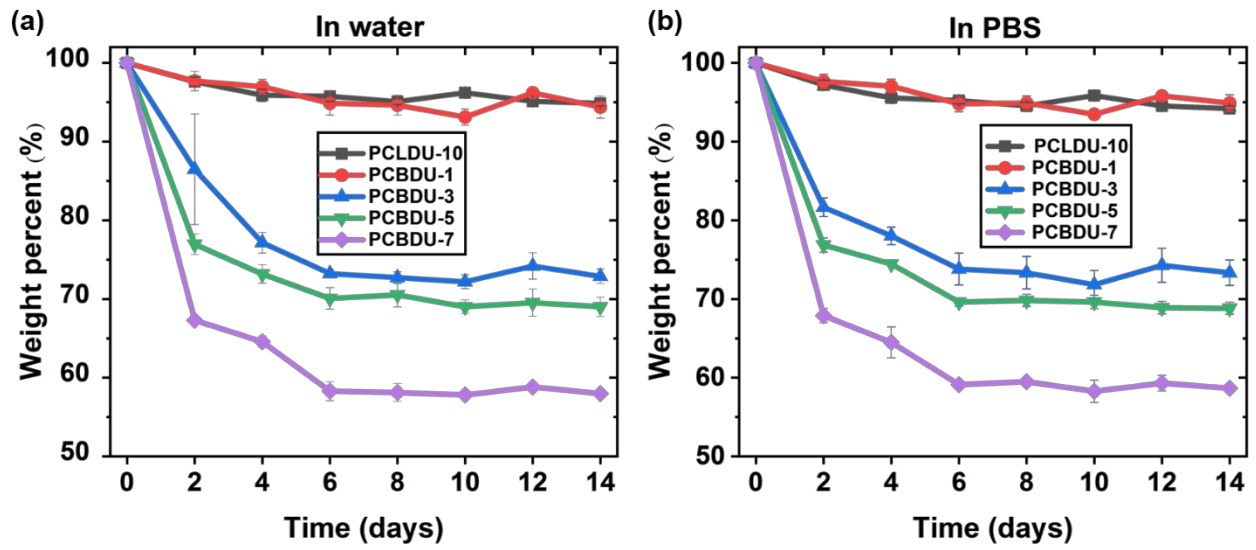


Figure 9. Hydrolytic degradation of PCBDU (a) in water and (b) in PBS as a function of time. PCLDU-10 was used as the control.

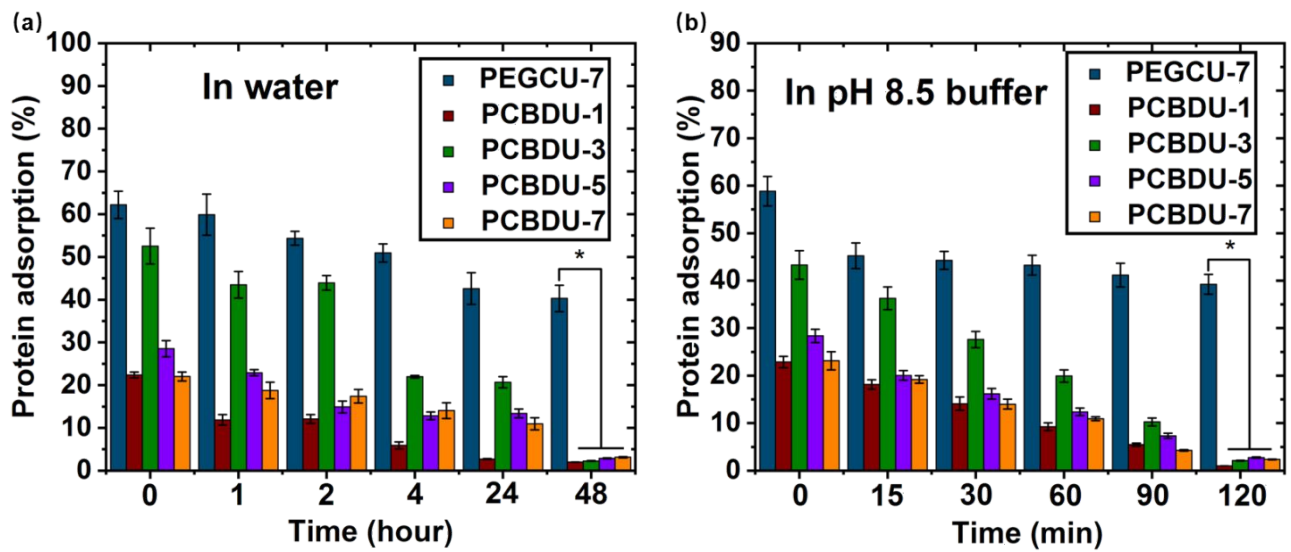


Figure 10. Protein adsorption of PCBDUs relative to the control (API-PU) with different hydrolysis times in (a) water and (b) pH-8.5 Tris buffer. ($n=3$, $p \leq 0.05$)

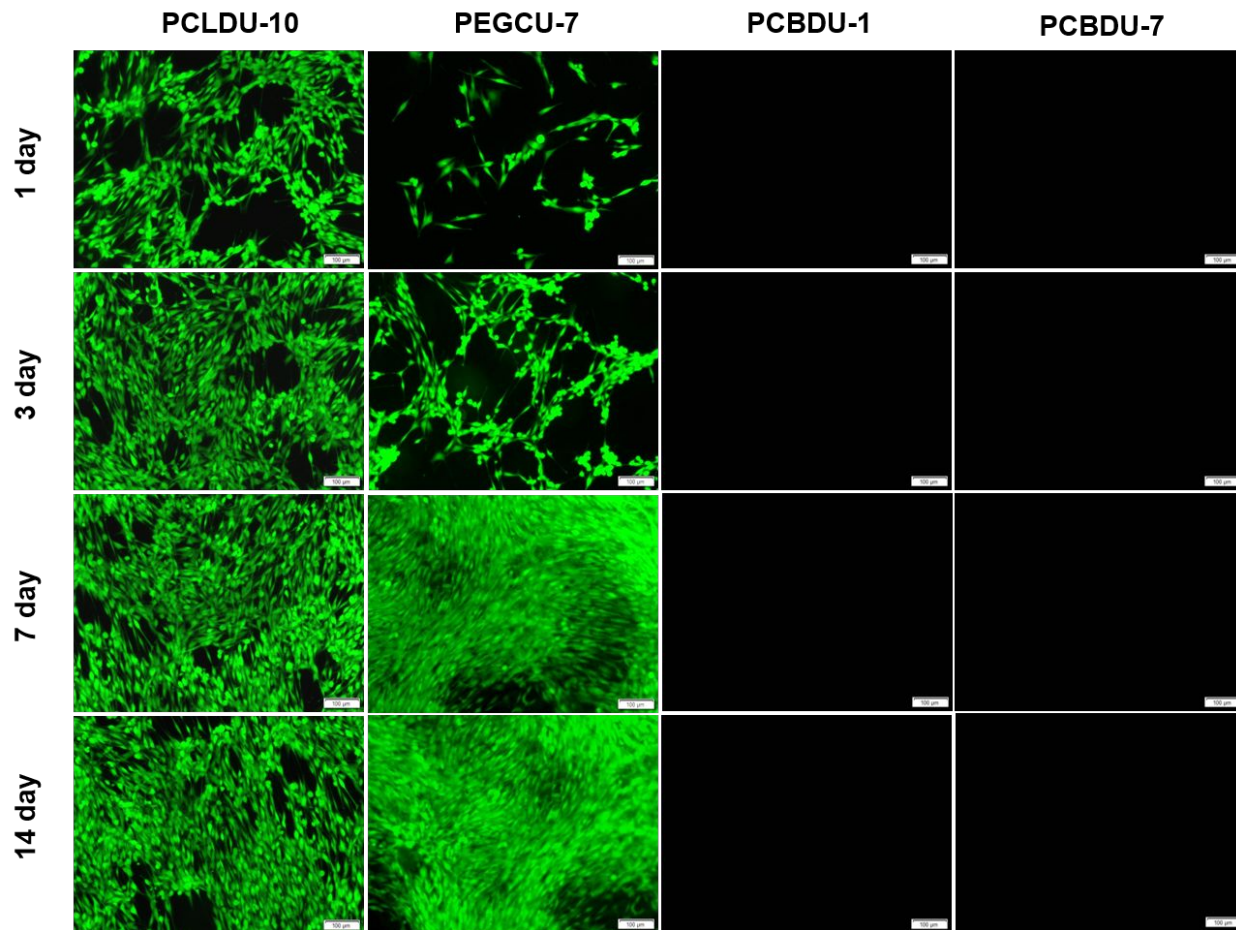


Figure 11. Images of the attachment of NIH-3T3 fibroblast cells on PCLDU-10, PEGCU-7, PCBUDU-1, and PCBUDU-7 after 1, 3, 7, and 14 days immersed in cell solution. The scale bar is 100 μm .